Received: 9 June 2023 | Revised: 17 January 2024 | Accepted: 3 February 2024

DOI: 10.1002/pip.3792

RESEARCH ARTICLE

PROGRESS IN PHOTOVOLTAICS WILEY

Implementation of nickel and copper as cost-effective alternative contacts in silicon solar cells

Veysel Unsur[1,2]

[1]Department of Fundamental Sciences, Necmettin Erbakan University, Konya, Turkiye

[2]Center of Solar Energy Research and Applications, ODTÜ-GÜNAM, Ankara, Turkiye

Correspondence
Veysel Unsur, Center of Solar Energy Research and Applications, ODTÜ-GÜNAM, Ankara, Turkiye.
Email: veysel.unsur@odtugunam.org

Funding information
Scientific and Technological Research Council of Turkiye, Grant/Award Numbers: 120E474, 122M311

Abstract

Efficient metal contact formation is pivotal for the production of cost-effective, high-performance crystalline silicon (Si) solar cells. Traditionally, screen-printed silver (Ag) contacts on the front surface have dominated the industry owing to their simplicity, high throughput, and significant electrical benefits. However, the high cost associated with using over 13–20 mg/Wp of Ag can impede the development of truly cost-effective solar cells. Therefore, there is an urgent need to explore alternative, economically viable metals compatible with silicon substrates. This study reports on the application of a contact stack consisting of Ag, nickel (Ni), and copper (Cu) in Si solar cells. To prevent Schottky contact formation, Ag is implemented as a seed layer, whereas Ni and Cu form the metal bulk layer. The fabricated bi-layer stack without selective emitter exhibits a maximum efficiency of ∼21.5%, a fill factor of 81.5%, and an average contact resistance of 5.88 $m\Omega \cdot cm^2$ for a monofacial PERC cell. Microstructure analysis demonstrates that the metals within the contacts remain distinct, and Cu diffusion into the silicon during the firing process is absent. Consequently, printed bi-layer contacts emerge as a promising alternative to Ag contacts, reducing the Ag consumption to below 2.5 mg/Wp per cell without compromising overall efficiency.

KEYWORDS
alternative metallization, copper contacts, LCOE, nickel contacts, screen printing, sensitivity analysis, Si solar cells

1 | INTRODUCTION

Screen-printed silver (Ag) metal contacts have long been favored in producing silicon (Si) solar cells because of their simplicity, maturity, and high throughput. Their dominance in the photovoltaic (PV) market is largely due to their excellent conductivity and solderability.[1–4] However, despite its advantages, the use of screen-printed Ag contacts has a high cost, contributing up to 40% of the total cell production expense, posing a major barrier to scaling and achieving cost-effective solar cells.[5–7] Consequently, there is a pressing need to investigate alternative metals that have the potential to form ohmic contacts with Si substrate while reducing overall production costs. Metals such as copper (Cu) and nickel (Ni) have been extensively explored because of their similar conductivity and significantly lower cost compared with Ag.[8–14] Techniques such as plating, including electroplating and light-induced plating, have emerged as promising methods for precise contact formation with these metals. However, the complexity of this process, including additional steps such as photoresist application,

laser opening of Ni or Cu deposition, and the use of large amounts of consumables, adds to the fabrication cost and deviates from current manufacturing practices.

To maintain efficiency without increasing costs, it is crucial to adopt a metallization process that aligns with the state-of-the-art in its simplicity and high throughput. Printable metal pastes derived from Cu or Ni offer a potential solution, provided they can be adapted for fire-through applications. Prior studies have experimented with low-temperature curable Cu alloys or floating busbar designs.[15–19] However, these methods necessitate additional laser contact openings at the front surface and are often only applicable to certain grid designs such as floating busbars. In addition, the use of high-temperature Cu pastes has been largely avoided because of Cu's aggressive diffusion even at room temperature, except for recent studies of the Cu fire-through pastes, though these have yet to match the efficiency of their Ag counterparts.[20] Furthermore, directly contacting alternative metals such as Ni onto the Si emitter can potentially limit a solar cell's power conversion efficiency because of adhesion problems, recombination losses, and contact resistance. To mitigate these issues, a seed layer capable of forming an ohmic-like contact with Si is often placed beneath the metal bulk.[10,21,22] Ag is an ideal candidate for this seed layer, owing to its established role in the industry and the compatibility of its metal work function with the Si substrate.

Despite the extensive exploration of Cu and Ni as alternatives to Ag in Si solar cells, this study introduces a novel approach by employing a screen-printable fire-through technique for these metals, both with and without the inclusion of glass frit. This work further distinguishes itself by providing a detailed investigation into the composition of in-house metal pastes and their performance relative to commercial Ag paste. Additionally, we uniquely examine the influence of peak temperature on the fill factor for different contact designs, offering a comprehensive evaluation through an array of electrical assessments, thereby contributing a significant advancement to the field. Here, in this study, we explore the fabrication of passivated emitter and rear contact (PERC) Si solar cells with stack contacts comprising of Ag seed layer topped with Ni and Cu bulk using screen printing. The use of three different in-house prepared fire-through pastes of Ag, Cu, and Ni is demonstrated here. These pastes are screen-printed on the front surface of PERC cells to form the front contacts. Employing bi-layer contact structures of Ag/Ni and Ag/Cu not only presents a potentially effective alternative to Ag counterparts for highly efficient solar cells but also results in significant cost reduction.

2 | EXPERIMENTAL DETAILS

In the present study, PERC solar cells were fabricated from silicon wafers possessing a resistivity of 2 Ω.cm. A silicon nitride (SiNx:H) layer with a thickness of 70 nm was deposited as an antireflection coating (ARC) layer on the front surface, and a 5-nm-thick aluminum oxide (AlO_X) layer along with a 75-nm-thick SiN_X:H layer were deposited on the rear side through plasma-enhanced chemical vapor deposition (PECVD). An aluminum (Al) contact was screen-printed on the back surface and subsequently dried at 200°C, followed by the application of front gridlines using distinct metal pastes.

The first of these was a commercially available Ag paste, used as a reference for subsequent comparisons. The second paste, an in-house Ag paste, was composed of Ag metal powder (~3-μm particle size), a glass frit, and an organic vehicle. The glass frit, prepared using the melt quenching method, was constituted of 30%–40% lead oxide (PbO), 25%–35% tellurium oxide (Te_2O), 22%–26% bismuth oxide (Bi_2O_3), 1%–5% silicon dioxide (SiO_2), 1%–2% zinc oxide (ZnO), 1%–2% tungsten oxide (WO_3), and 1%–2% magnesium oxide (MgO). The organic vehicle contained terpineol ($C_{10}H_{18}O$) and texanol ($C_{12}H_{24}O_3$) as solvents, ethyl cellulose and polyvinylpyrrolidone (PVP) as binders, hydrogenated castor oil as a thixotropic agent, and sorbitan-triolate as a surfactant. These components were blended in a weight ratio of 82.5:3.5:14, respectively, and the resulting mixture was subjected to three-roll milling for 60 min for proper dispersion.

The third paste employed was a Nickel (Ni) paste, prepared both with and without the aforementioned glass frit. The Ni paste, which included the glass frit, was prepared using the same glass frit and organic vehicle as the in-house Ag paste but with a different weight ratio of components (77:3.5:19.5 for the Ni metal powder, glass frit, and organic vehicle, respectively). The Ni paste without the glass frit was prepared by combining Ni metal powder (4-μm particle size) with the same organic vehicle in a weight ratio of 85:15.

Finally, a copper (Cu) paste was prepared without glass frit. It contained the same organic vehicle and was mixed in a weight ratio of 88:12 with Cu metal powder with 1-μm particle size.

Upon fabrication, the commercial Ag paste (Heraeus SOL9661) was applied to identical M2 wafers (with 90 Ω/sq resistivity) to serve as a reference contacting mechanism. Other wafers of the same type were printed with the in-house Ag paste (single layer), in-house Ni paste (single layer), and stacks of Ag paste + Ni paste and Ag paste + Cu paste. Distinct screens were employed for each type of contact. For the bi-layer deposition and single-layer contacts, a coarser screen with 430/13 mesh/wire, 12–20-μm EOM thickness, and a 40-μm opening (S-1) was chosen to facilitate thicker metal deposits/A finer screen with 520/13 mesh/wire, 8–12-μm EOM thickness, and a 22-μm opening (S-2) was utilized for the seed layer Ag paste application. To measure the saturation current density and one of its components, $J_{0,\ metal}$, according to Fellmenth et al.,[23] a special grid pattern containing different metal fractions is printed on a symmetrical sample divided into 4-cm^2 area cell size.

Following the preparation and printing of the different contact materials onto the wafers (see the process flow in Figure 1), a co-firing process was executed using an atmospheric six-zone conveyor infrared (IR) belt furnace, adhering to the firing profiles outlined in Figure 1. An exploration of various peak temperatures was conducted at a constant belt speed of 230 in. per minute (ipm) to understand the influence of peak temperature on the fill factor (FF) for different contact designs. Rapid rates of temperature increase and decrease were employed, as detailed in the inset graph of Figure 1, in order to ensure

uniform formation of the back surface field (BSF) on the rear side and to enhance metal crystallite formation beneath the front contacts.

Upon completion of the firing process, the resulting solar cells underwent an array of electrical and optical assessments. Electrically, Suns-V_{OC} measurements were performed to investigate resistive effects, ideality factor (n), and saturation current density (J_0). Light current–voltage (I–V) measurements were carried out to ascertain the maximum power, as well as the open circuit voltage (V_{OC}) and fill factor (FF). Optically, the fabricated cells were examined via a scanning electron microscope (SEM) integrated with energy-dispersive X-ray (EDX) spectroscopy to visualize the cross-section between the metal contacts and the emitter region of the solar cells.

3 | RESULTS AND DISCUSSIONS

3.1 | Print quality

Table 1 shows the width and height of the single and bi-layer contacts before and after the firing in which the average finger widths fall within the range of 51 to 55 µm. Post-firing, the width of the contacts slightly shrunk except for Ag + Cu bi-layer stack that expanded to 56 µm because of the most likely ductile behavior of copper. Although the widths of the fingers shrink for each contact type, there is no ghost finger formation on the surface after the firing process, as shown in Figure 2. The single Ni contact exhibits the narrowest average width of 47 µm post-firing, having commenced at 55 µm prior to the firing process. This highlights the increased tendency for Ni fingers to sinter and compact, forming a continuous line. In comparison, the width of the conventional screen-printed single Ag contacts printed with S2 is slightly narrower because of a more established paste composition. However, the metal fractions of the contacts, which are related to glass frit used in this study, are similar, measuring 5.1% for commercial Ag, 5% for in-house Ag, 5.4% for the Ag + Ni bi-layer, and 5.7% for the Ag + Cu bi-layer, respectively. These are closely aligned with the approximated 5% metal fraction of commercial Ag contacts.[24,25] As also tabulated in Table 1, the width of the fingers varies depending on the metal used, a phenomenon potentially attributable to disparities in wetting and concentration within each paste. Therefore, there is a learning curve for in-house pastes to follow the industry standard finger width of below 20 µm. It is also important to note here that the metal paste composition, the screen stability, and the high accuracy of alignment play a role in reducing the finger width of double printing to industry standard. As for the metal composition, the in-house prepared pastes show promising results to achieve finer gridlines. However, the alignment factor and screen stability depend on the printing industry. For the finger height, contact with in-house prepared Ag paste gives the tallest finger,

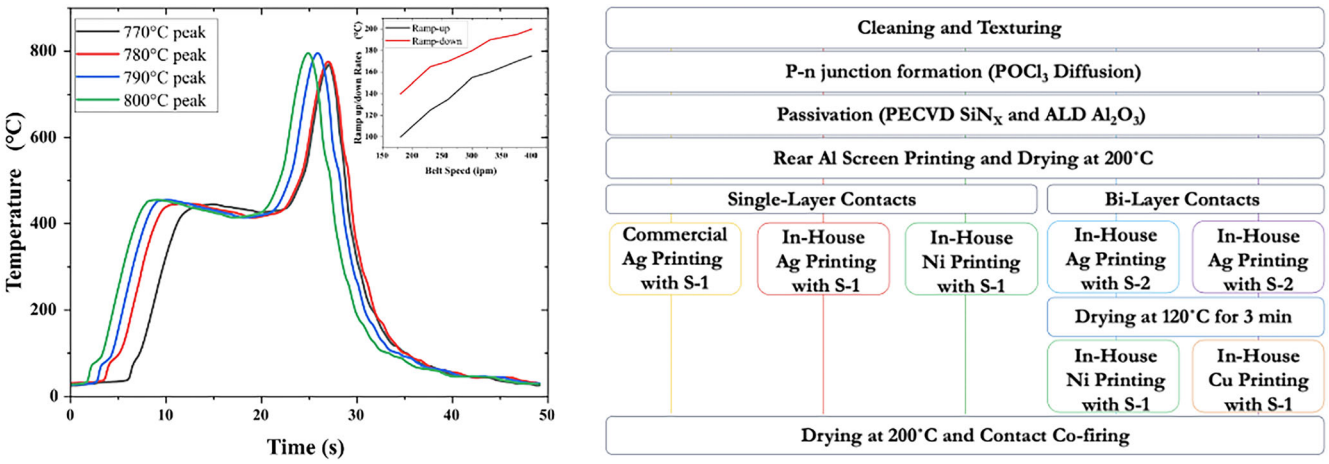

FIGURE 1 (Left) The contact co-firing temperature profiles with different peak temperatures. The inset graph shows the temperature velocity of the conveyor belt furnace for the profiles. (Right) The process flow of the solar cells with different contact types (S1 refers to screen 1 and S2 refers to screen 2).

TABLE 1 The average finger widths and height before and after contact co-firing process.

Contacts	Finger width before firing (µm)	Finger width after firing (µm)	Finger height after firing (µm)
Ag (reference)	53	49	9
Ag (in-house)	52	50	14
Ni	55	47	9
Ag + Ni	51	51	13
Ag + Cu	55	56	10

which suggests that the surfactant and thixotropic agent used in the paste, although the same type is used in each paste, correlate with Ag particles better than the others. The height of the Ag seed layer in Ag + Ni and Ag + Cu was around 2 μm because of the lower snap-off distance used to obtain flat-top contact. Thus, the height of the bi-layer contacts is not significantly higher than single-layer contacts.

3.2 | Contact and line resistances

Supporting the above-mentioned premise, the results of finger resistance (R_F) for the single-layer Ni contact compared with the single-layer Ag contact across different firing profiles, as depicted in Figure 3a, demonstrate promising outcomes. Particularly, screen-printed Ni contacts at the industry-standard peak temperature of around 770–800°C (on the sample) exhibit favorable results in finger resistance compared with Ag counterparts. The R_F shows limited deviation with varying contact co-firing peak temperatures, suggesting that metal particle sintering occurs properly for both Ni and Ag contacts. This can potentially be attributed to the softening of Ni metals at the intersection of Ni/Si, predominantly occurring at elevated temperatures. Comparing the contact resistance of two single-layer contacts, on the other hand, proves that Ag makes better contact with Si than Ni, as seen in Figure 3b. This advantage stems from Ag's lower metal's work function compared with Ni. The closer alignment of Ag's work function with Si's electron affinity (~4.05 eV) facilitates efficient charge carrier transfer across the metal–semiconductor interface, thereby reducing contact resistivity. Additionally, the relatively low contact resistance observed for both contact types suggests that the in-house prepared glass frit is effectively etching the ARC layer without damaging the emitter. This is further supported by the power conversion efficiency and fill factor (FF) results of both single-layer contacts, as shown in Figure 4. In line with the result of resistivity measurements of the contacts, the FF and the efficiency for Ni contacts suffer because of high series resistance thereby underscoring the potential of Ag as a viable seed layer.

3.3 | I-V characteristics

To overcome the high contact resistivity of Ni and reduce the high cost of Ag contacts, Ag is used as a seed layer with Ni and Cu forming the bulk of the metal in a bi-layer contact type. The average electrical output parameters and the Suns-V_{OC} measurement results for the

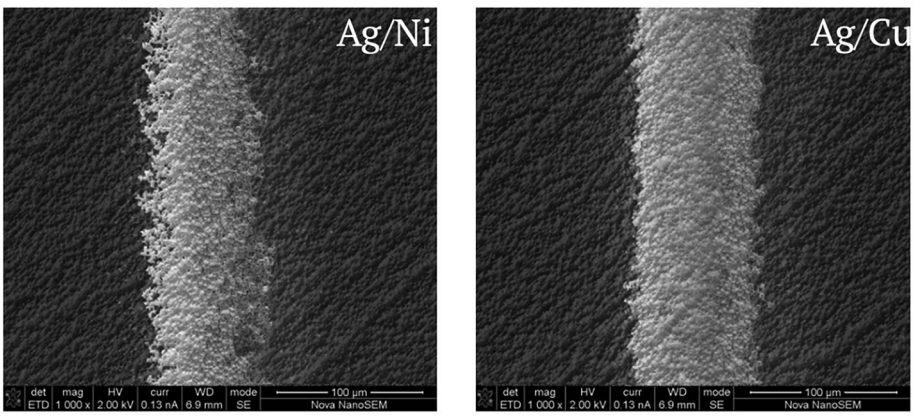

FIGURE 2 Top view SEM images of the two bi-layer stack contacts after firing.

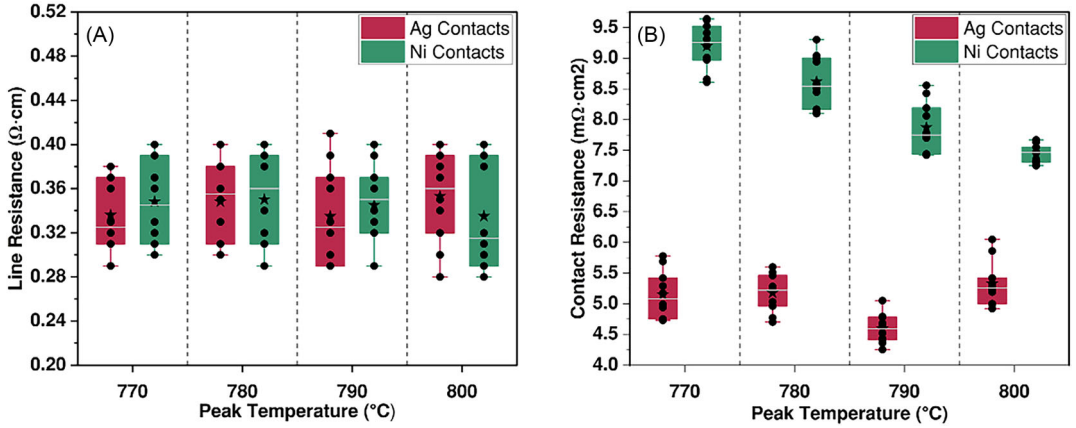

FIGURE 3 The finger and contact resistance measurements according to different peak temperatures of contact co-firing for Ag and Ni contacts.

single layer, along with bi-layer contact types, are presented in detail with respect to their optimized firing temperature in Table 2. For reference, a screen-printed Ag contact solar cell is presented in Table 3. The in-house prepared Ag paste performs the best among the other types with an average efficiency of 21.7%. The second best performing structure is Ag/Cu bi-layer contact stack, which achieves 21.32% efficiency and FF of 81.4%. This result implies that even though the samples are fired at a peak temperature of 770°C, there is no Cu contamination in the cell, as supported by high shunt resistance (R_{SH}) values of 150 000. The $J_{0,\ metal}$ value of 480 fA/cm^2 and the R_C of 5.88 mΩ·cm^2 for the Ag/Cu contact, compared with reference Ag contact of 510 fA/cm^2 and 4.63 Ω·cm^2, also strongly indicate that Ag is successfully blocking the Cu diffusion into the junction. The total series resistance (R_S) of the same contact, obtained by the light IV measurement, on the other hand, shows an additional resistive effect that may be due to the line resistance of the stack contact as a whole or it could arise from the reduction of pFF caused by contamination. This conclusion is further substantiated by the microstructure analysis depicted in Figure 5. The elemental examination reveals that the Cu remains on top of the Ag layer, indicating that Cu, despite its aggressive diffusion properties, has not permeated underneath the Ag. The Ag/Ni contacts also result in promising electrical performance. The FF of 81.2% indicates that the contact formation is complete and there is no shunt in the cell considering the contact stack of Ag/Ni yielded close to maximum shunt resistance. However, the contact resistance and total series resistance are slightly higher than the others, possibly because of some lift-off from the substrate between Ag + Ni and Si. For the Ni as a single contact, in addition to the above-mentioned analysis, the cell is clearly shunted and degraded because of the use of the same glass frit in each paste and the peak firing temperature of 800°C, which is clearly pushing the contact proximity closer to the junction. This is supported by the low shunt resistance of 12 050 Ω·cm^2.

3.4 | Microstructural analysis

Challenges in the printing process manifest themselves in two distinct forms: lift-off of Ag/Ni stack from the front surface and delamination of Ag/Cu contacts between the Ag and Cu. As illustrated by SEM images, these issues not only compromised the mechanical stability of the contacts but also influenced their electrical performance.

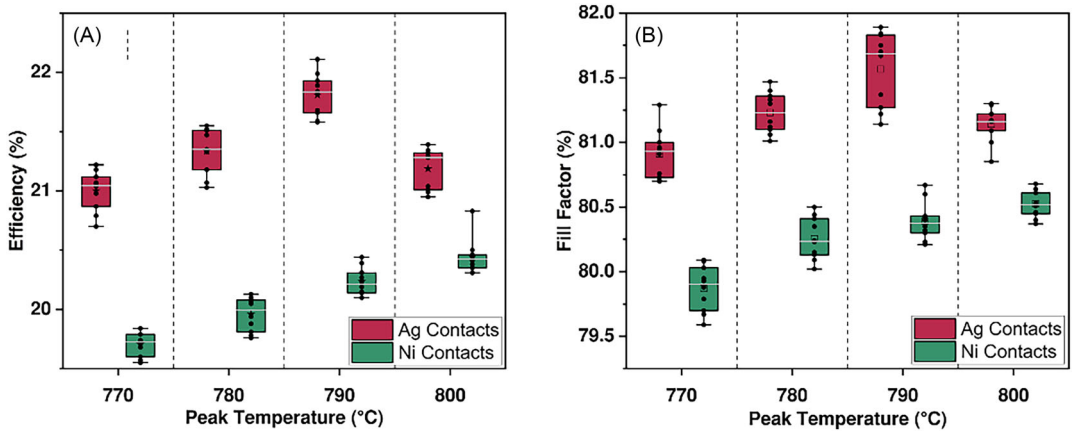

FIGURE 4 The efficiency and fill factor measurements according to different peak temperatures of contact co-firing for Ag and Ni contacts.

TABLE 2 The average electrical output parameters of best-performed cells with respect to peak temperature.

Metal stack	V_{OC} (mV)	*FF* (%)	η (%)	R_s (Ω·cm^2)	R_c[a] (mΩ·cm^2)	$J_{0,\ metal}$ (fA/cm^2)	R_{SH} (kΩ·cm^2)	Peak (°C)
Ag	665	81.7	21.72	0.54	4.63	510	150	790
Ag/Ni	661	81.2	21.14	0.76	6.41	530	131	780
Ag/Cu	663	81.4	21.32	0.65	5.88	480	150	770
Ni	654	80.1	20.44	0.84	7.42	980	12	800

[a]The contact resistivity for each type is calculated with the effective width of the bi-layer contacts (Ag + Ni or Ag + Cu).

TABLE 3 The electrical output parameters of a screen-printed Ag contacted reference cell.

Type	V_{OC} (mV)	*FF* (%)	η (%)	R_s (Ω·cm^2)	R_C (mΩ·cm^2)	$J_{0,\ metal}$ (fA/cm^2)
Reference Ag contacts	667	81.6	21.9	0.51	4.11	410

Figure 6a provides a cross-sectional SEM image of an Ag/Cu contact after undergoing a contact co-firing process at 780°C. The clear separation between the Ag and Cu layers might be attributable to the differential thermal expansion of these metals during the firing process. However, this delamination issue is not apparent in contacts co-fired at peak temperatures below 780°C, underlining the significance of optimal firing conditions for the stability of these bi-layer contacts. The SEM image in Figure 6b exhibits a lift-off scenario with the Ag/Ni stack, where the contact stack detaches from the Si substrate in the middle, whereas the remaining intact at the edges. This occurrence could stem from multiple factors, including differential thermal expansion, interfacial reactions, and inadequate surface preparation, among others. These observations align with a previous study,[26] which reported similar lift-off and delamination issues in aerosol printed bi- and tri-stack layers of Ag frit/Ni and Ag frit/Ni/Cu when fired above 790°C peak firing temperature.

The efficiency and series resistance parameters, plotted based on finger width associated with lift-off and delamination in stacked contacts, are presented in Figure 7. The results show that bi-layer contacts perform similarly to Ag counterparts, providing no delamination or a lift-off occurs in the structure. Lift-off from the center damages the performance to the extent that the efficiency of the Ag/Ni contacted cell may drop to as low as 16.62%, as shown by the highlighted data points in Figure 7 (left). The series resistance of those cells, shown in Figure 7 (right), may exceed 1 $\Omega \cdot cm^2$ because of high contact resistance, whereas delamination presents itself as a finger resistance and increases the R_S for the Ag/Cu contacts. For those cells where the contact layers are intact, the contact resistance is in the range of the Ag reference, implying that the performance can reach industry standards and lower the Ag usage per watt. Following these data, it can be concluded that the performance of both Ag/Cu and Ag/Ni contacts closely mirrors that of their Ag counterparts. These findings suggest a high potential for these bi-layer configurations to serve as effective alternatives to Ag. By leveraging these alternatives, a considerable reduction in Ag consumption per watt can be achieved without compromising the efficiency of solar cells.

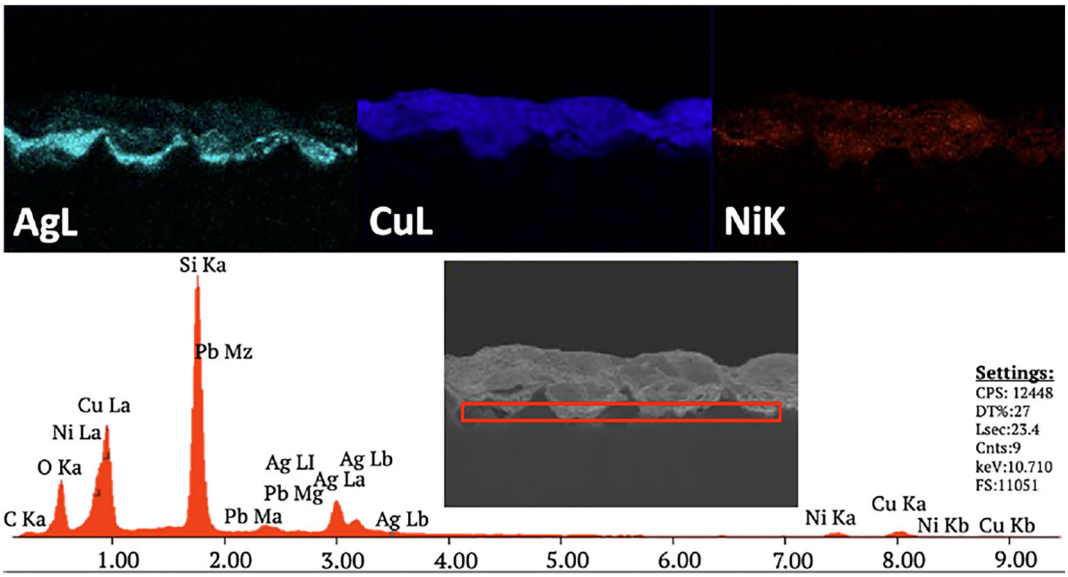

FIGURE 5 Cross-section elemental X-ray analysis of Ag/Cu contacts.

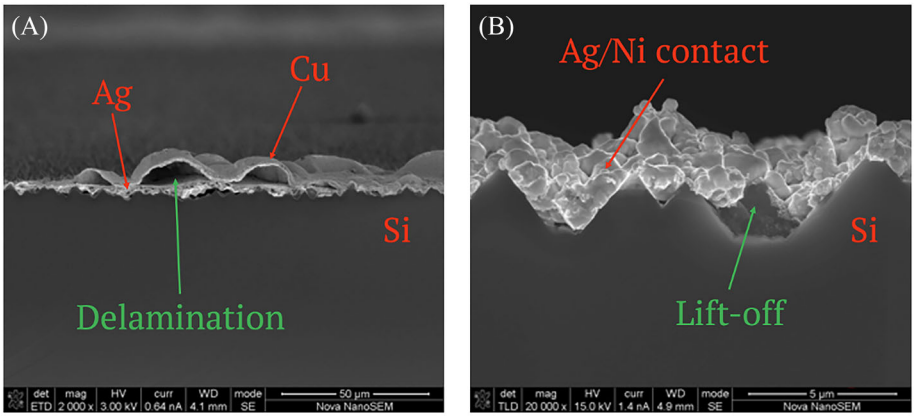

FIGURE 6 (a) SEM image of the Ag/Cu bi-layer stack contacts after contact co-firing, the metals detached from each other created high line resistance, and (b) SEM image of the Ag/Ni contact lifts off from the Si substrate.

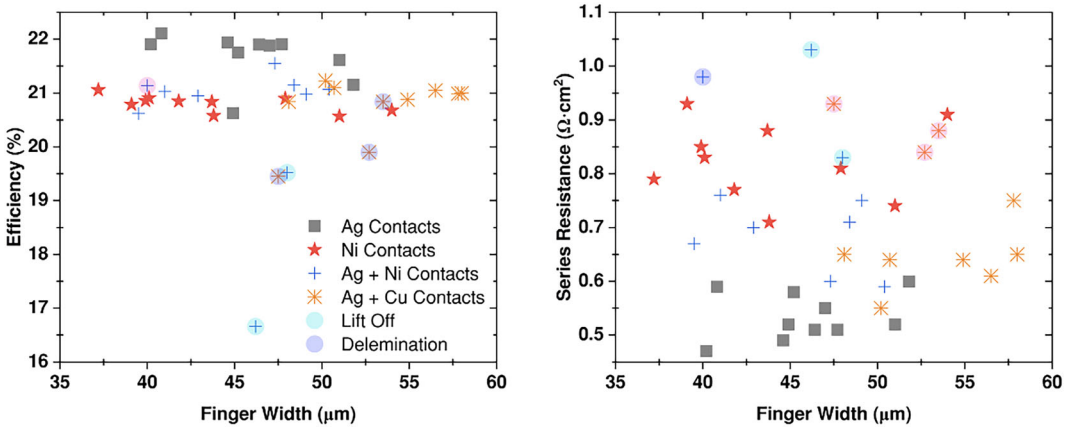

FIGURE 7 The efficiency and series resistance for different contacts with different finger widths. Highlighting on the data point shows if the contact has a lift-off or delamination; green highlight means lift-off from the substrate, and pink means interlayer delamination.

3.5 | Mechanical properties

Peel force tests were conducted to assess the mechanical robustness of the proposed alternative contacts, both single and bi-layer. These tests involved peeling the soldered ribbons from the busbars at angles of 90° and 180°. The results, presented in Figure 8, indicate that the commercial Ag paste exhibited average peel forces of 4.4 and 4.9 N/mm at 90° and 180°, respectively. In comparison, the in-house prepared Ag paste demonstrated a slightly improved performance at 90° with an average peel force of 4.6 N/mm while maintaining comparable strength at 180°.

In the case of the single-contacted Ni paste, the adhesion to the substrate was notably weaker averaging around 3 N/mm. This can be attributed to the absence of NiSi formation, as no annealing was applied around 450°C, which is essential to form the NiSi phases at the cross-section. Consequently, the Ni contacts exhibited the lowest peel force among the samples tested.

For bi-layer contacts comprising Ag + Ni and Ag + Cu, the peel force measurements were similar to those of the reference Ag-contacted cells. The maximum peel force of 6 N/mm is read from the Ag + Ni contacts, and Ag + Cu contacts yield over 5 N/mm. However, it is critical to highlight that samples exhibiting lift-off and delamination, specifically for Ag + Ni and Ag + Cu contacts, were outliers in these tests. These samples demonstrated significantly lower peel forces, measuring 1.8 N/mm for Ag + Ni and 2.3 N/mm for Ag + Cu at a 90° peel angle. This observation underscores the importance of achieving optimal layer cohesion in bi-layer contact fabrication to ensure mechanical integrity.

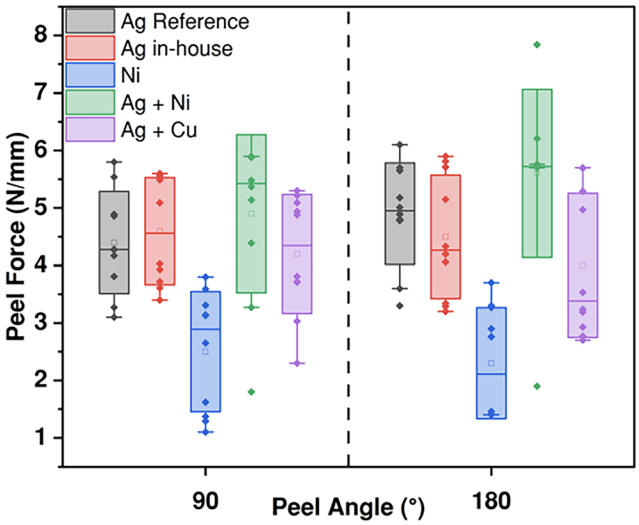

FIGURE 8 The peel force test measurements for different types of contacts.

3.6 | Cost and sensitivity analysis

One of the key determinants of the viability and scalability of the proposed alternative metallization technique is its cost-effectiveness and potential impact on the levelized cost of electricity (LCOE). Prior research by Zhang[27] demonstrated that in traditional solar cell manufacturing, Ag consumption is around 13–20 mg per watt-peak (mg/Wp). This represents a significant cost because of the high market price of Ag, thereby posing a potential barrier to terawatt-scale production. In order to calculate the reduction in silver usage achieved through the employment of a bi-layer structure, using Ag as a seed layer and either Ni or Cu as bulk metal, all cells were weighed before printing and after co-firing the contacts, ensuring the complete removal of solvents and binders. The metallization patterns for each contact type were maintained consistent with 110 fingers and 5 busbars. The cells weighed for metal consumption analysis were carefully selected based on the average finger width to minimize discrepancies between samples. The bi-layer contacts for consumption analysis underwent a two-step firing process: once after Ag printing and once after Ni or Cu printing. This allowed for accurate determination of Ni and Cu consumption. As Table 4 illustrates, the average values of Ag, Ni, and Cu consumption for the completed cells demonstrate that Ag consumption for bi-layer contacts is below 2.5 mg/Wp. This

	Ag reference cell	Ag/Ni contacted cell	Ag/Cu contacted cell
Ag consumption	91.5 mg–13.07 mg/Wp	16.4 mg–2.41 mg/Wp	15.9 mg–2.31 mg/Wp
Ni consumption	-	41.15 mg–6.04 mg/Wp	-
Cu consumption	-	-	44.9 mg–6.51 mg/Wp

TABLE 4 Ag, Ni, and Cu consumption of the finished cells after contact co-firing.

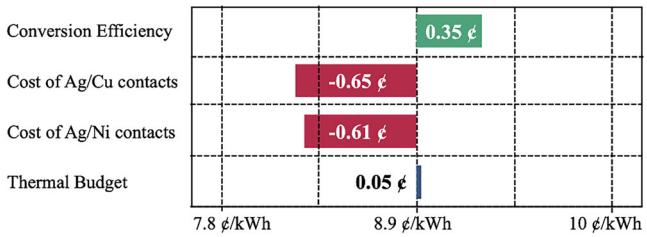

FIGURE 9 Sensitivity analysis of the LCOE for solar cells with bi-layer contact structure.

represents nearly a sevenfold reduction when compared with the Ag-contacted reference cell. Considering the Ag price of $808, Ni price of $24, and Cu price of $8, the metallization cost per wafer drops 80.75% lower for Ag/Ni contacts and 82.15% for Ag/Cu contacts. The reflection of this cost drop on the LCOE is calculated according to Lazard's calculation[28] with System Advisor Model (SAM) by NREL in a scenario in which it is assumed that M2-sized solar cells are used for 1GW solar farm in south Turkiye where the solar insolation is 5.1 kWh/m^2/day. The results show that, for reference, Ag-contacted solar cells yield an LCOE of 8.9¢/kWh. To analyze the effect of the bi-layer contacted cells on the LCOE, the sensitivity analysis is carried out in which the inputs are varied according to their electrical output parameters and metal consumption given in Tables 2 and 4, respectively. Figure 9 shows the sensitivity analysis results where a negative correlation (to the left from the centerline) means lower LCOE and a positive correlation (to the right from the centerline) results in higher LCOE. It is illustrated in Figure 9 that although the loss in power conversion efficiency due to high series resistance has an impact on increasing the LCOE of around 0.35¢/kWh, the cost drop of metal consumptions has a higher impact on lowering the LCOE of around 0.65¢/kWh. The increase in thermal budget for the contact firing of bi-layer contacts has a limited effect on the LCOE. Therefore, the financial implications of adopting this bi-layer metallization approach are significant. The drastically reduced silver consumption leads to substantial cost savings, which are directly reflected in the LCOE.

4 | CONCLUSION

In conclusion, adopting the proposed alternative metallization technique, employing a screen-printed bi-layer configuration with either Ag/Ni or Ag/Cu, presents significant advantages in terms of cost-effectiveness. These configurations, while maintaining a similar level of performance as traditional Ag contacts, substantially reduce the silver consumption and, hence, the overall metallization cost per wafer. Importantly, these cost savings are reflected in the LCOE, showcasing the potential of this alternative technique to bring about notable cost efficiencies in the solar power industry. Although the efficiency loss due to higher series resistance and the slight increase in thermal budget for contact firing of bi-layer contacts are to be taken into account, the reduction in metal costs substantially outweighs these factors, resulting in a lower LCOE. Lastly, the peel force tests result in favor of the long-term sustainability of the contacts. This innovative approach, combining enhanced performance with economic viability, has the potential to significantly advance the manufacturing process of solar cells and bolster the broader transition toward more sustainable and cost-effective energy solutions.

ACKNOWLEDGEMENTS

The authors would like to express their profound gratitude for the support provided by the Scientific and Technological Research Council of Turkiye (TÜBİTAK). This research has been made possible through grants under reference numbers 120E474 and 122M311.

DATA AVAILABILITY STATEMENT

The data that support the findings of this study are available on request from the corresponding author. The data are not publicly available due to privacy or ethical restrictions.

ORCID

Veysel Unsur https://orcid.org/0000-0002-5942-4129

REFERENCES

1. Unsur V, Chen N, Ebong A. A mathematical investigation of the impact of gridline and busbar patterns on commercial silicon solar cell performance. *J Comput Electron*. 2020;19(2):854-865. doi:10.1007/s10825-020-01455-z
2. Haigh AD Fired through Printed Contacts on Antireflection Coated Silicon Solar Cells, 1976.
3. Schubert G, Huster F, Fath P. Physical understanding of printed thick-film front contacts of crystalline Si solar cells—review of existing models and recent developments. *Solar Energy Mater Solar Cells*. 2006;90(18–19):3399-3406. doi:10.1016/j.solmat.2006.03.040
4. Ralph EL Recent advancements in low cost solar cell processing. in 11th Photovoltaic Specialists Conference, 1975, p. 315.
5. Hallam B, Kim M, Zhang Y, et al. The silver learning curve for photovoltaics and projected silver demand for net-zero emissions by 2050. *Prog Photovolt Res Appl*. 31(6):598-606. doi:10.1002/pip.3661
6. Branker K, Pathak MJM, Pearce JM. A review of solar photovoltaic levelized cost of electricity. *Renew Sustain Energy Rev*. 2011;15(9):4470-4482. doi:10.1016/j.rser.2011.07.104
7. Verlinden PJ. Future challenges for photovoltaic manufacturing at the terawatt level. *J Renew Sust Energy*. 2020;12(5):053505. doi:10.1063/5.0020380

8. Limodio G, de Groot Y, van Kuler G, et al. Copper-plating metallization with alternative seed layers for c-Si solar cells embedding carrier-selective passivating contacts. *IEEE J Photovolt*. 2019;10(2):372-382. doi:10.1109/JPHOTOV.2019.2957671
9. Mette A, Richter PL, Hörteis M, Glunz SW. Metal aerosol jet printing for solar cell metallization. *Progr Photovolt Res Appl*. 2007;15(7):621-627. doi:10.1002/pip.759
10. Glunz S, Mette A, Alemán M, Richter P, Filipovic A, Willeke G New concepts for the front side metallization of silicon solar cells. in *21st European photovoltaic solar energy conference and exhibition*, 2006, p. 8.
11. Glunz SW, Aleman M, Bartsch J, *et al*., "Progress in advanced metallization technology at Fraunhofer ISE," in *2008 33rd IEEE Photovoltaic Specialists Conference*, May 2008, pp. 1–4. doi:10.1109/PVSC.2008.4922746.
12. Rehman AU, Lee SH. Review of the potential of the Ni/Cu plating technique for crystalline silicon solar cells. *Materials*. 2014;7(2):1318-1341. doi:10.3390/ma7021318
13. Raval MC, Solanki CS. Review of Ni-Cu based front side metallization for c-Si solar cells. *J Solar Energy*. 2013;2013:20.
14. Akgayev B, Sezgin A, Yilmaz M, Unsur V. Screen printable fire through nickel contacts for silicon solar cells. *Solar Energy Mater Solar Cells*. 2023;261:112528. doi:10.1016/j.solmat.2023.112528
15. Yoshida M, Tokuhisa H, Itoh U, Kamata T, Sumita I, Sekine S. Novel low-temperature-sintering type Cu-alloy pastes for silicon solar cells. *Energy Procedia*. 2012;21:66-74. doi:10.1016/j.egypro.2012.05.009
16. Wood D, Kuzma-Filipek I, Russell R, et al. Non-contacting busbars for advanced cell structures using low temperature copper paste. *Energy Procedia*. 2015;67:101-107. doi:10.1016/j.egypro.2015.03.293
17. Nakamura K, Takahashi T, Ohshita Y. "Novel silver and copper pastes for n-type bi-facial PERT cell," in *31st European Photovoltaic Solar Energy Conference and Exhibition*, 2015, pp. 536–539.
18. Chen N, Rudolph D, Peter C, et al. Thermal stable high-efficiency copper screen printed back contact solar cells. *Solar RRL*. 2023;7(2):2200874. doi:10.1002/solr.202200874
19. Rudolph D, Farneda R; Timofte T *et al*., "Screen printable, non-fire-through copper paste applied as busbar metallization for back contact solar cells," presented at the PROCEEDINGS OF THE 10TH WORKSHOP ON METALLIZATION AND INTERCONNECTION FOR CRYSTALLINE SILICON SOLAR CELLS, Genk, Belgium, 2022, p. 020006. 10.1063/5.0127359.
20. Huneycutt S, Ebong A, Ankireddy K, Dharmadasa R, Druffel T. "Understanding the Solar Cell Contacts With Atmospheric Screen-printed Copper," in 2022 IEEE 49th Photovoltaics Specialists Conference (PVSC), IEEE, 2022, pp. 0937–0940.
21. Raval MC, Solanki CS. Characterization of electroless nickel as a seed layer for silicon solar cell metallization. *Bull Mater Sci*. 2015;38(1):197-201. doi:10.1007/s12034-014-0828-1
22. Limodio G, de Groot Y, van Kuler G, et al. Copper-plating metallization with alternative seed layers for c-Si solar cells embedding carrier-selective passivating contacts. *IEEE J Photovolt*. 2020;10(2):372-382. doi:10.1109/JPHOTOV.2019.2957671
23. Fellmeth T, Born A, Kimmerle A, Clement F, Biro D, Preu R. Recombination at metal-emitter interfaces of front contact technologies for highly efficient silicon solar cells. *Energy Procedia*. 2011;8:115-121. doi:10.1016/j.egypro.2011.06.111
24. Padhamnath P, Buatis JK, Khanna A, et al. Characterization of screen printed and fire-through contacts on LPCVD based passivating contacts in monoPoly™ solar cells. *Solar Energy*. 2020;202:73-79. doi:10.1016/j.solener.2020.03.087
25. Li M, Wong J, Chen N, Aberle AG, Stangl R. Determination of metallization-induced recombination losses of screen-printed silicon solar cell contacts and their dependence on the doping profile. *IEEE J Photovolt*. 2018;8(6):1470-1477. doi:10.1109/JPHOTOV.2018.2866177
26. Unsur V, Klein T, van Hest MF, Al Jassim M, Ebong A. Rapid thermal processing of cost-effective contacts for silicon solar cells. *Prog Photovolt Res Appl*. 2019;27(5):453-459. doi:10.1002/pip.3119
27. Zhang Y, Kim M, Wang L, Verlinden P, Hallam B. Design considerations for multi-terawatt scale manufacturing of existing and future photovoltaic technologies: challenges and opportunities related to silver, indium and bismuth consumption. *Energ Environ Sci*. 2021;14(11):5587-5610. doi:10.1039/D1EE01814K
28. Ray D Lazard's Levelized Cost of Energy Analysis—Version 16.0, p. 21, 2023.

How to cite this article: Unsur V. Implementation of nickel and copper as cost-effective alternative contacts in silicon solar cells. *Prog Photovolt Res Appl*. 2024;32(4):267-275. doi:10.1002/pip.3792